Hysteresis phenomena and multipulse formation of a dissipative system in a passively mode-locked fiber laser

Xueming Liu
State Key Laboratory of Transient Optics and Photonics, Xi'an Institute of Optics and Precision Mechanics, Chinese Academy of Sciences, Xi'an 710119, People's Republic of China
(Received 14 November 2009; published 12 February 2010)

A model describing the dissipative soliton evolution in a passively mode-locked fiber laser is proposed by using the nonlinear polarization rotation technique and the spectral filtering effect. It is numerically found that the laser alternately evolves on the stable and unstable mode-locking states as a function of the pump strength. Numerical simulations show that the passively mode-locked fiber lasers with large net normal dispersion can operate on multiple pulse behavior and hysteresis phenomena. The experimental observations confirm the theoretical predictions. The theoretical and experimental results achieved are qualitatively distinct from those observed in net-anomalous-dispersion conventional-soliton fiber lasers.

DOI: 10.1103/PhysRevA.81.023811 PACS number(s): 42.55.Wd, 42.81.Dp, 42.65.Tg, 42.65.Re

I. INTRODUCTION

Passively mode-locked (PML) fiber lasers have been extensively investigated because they are able to easily generate self-starting short pulses [1–6]. Generally, the passive mode-locking techniques used in mode-locking lasers have a nonlinear loop mirror [4], nonlinear polarization rotation (NPR) [7], and a semiconductor saturable absorber [8]. When a fiber laser is made of fibers with purely anomalous group velocity dispersion (GVD) or net anomalous GVD, "sech-profile" pulses with spectral sidebands can be formed as a result of the balance between anomalous GVD and positive nonlinearity. However, the soliton energy quantization effect limits the lasers to produce optical pulses with larger pulse energy and narrower pulse width [9,10]. As a consequence, multiple-soliton pulses are always generated in the laser cavity and they usually have the same pulse energy and pulse width [9–11].

Solitons are ubiquitous in nature and occur in various physical systems [11–14]. Conventional solitons in conservative systems result from the balance between the dispersion (or diffraction) and the nonlinearity of the material. Dissipative solitons (DSs) exist in nonconservative systems [13] and, hence, their dynamics is markedly different from that of conventional solitons. The gain and loss coexisting in the dissipative system play essential roles in the generation of DSs [14,15]. A laser with purely positive GVD (or large net-normal GVD) would presumably have to exploit dissipative processes to a greater degree in the steady-state pulse shaping [16]. Even the DSs can be realized in lasers operating in the anomalous dispersion regime [17,18].

Recently, multipulse operation in PML fiber lasers was numerically simulated and experimentally observed. Tang *et al.* had proposed that the formation of multiple solitons in the laser is caused by a peak-power-limiting effect of the laser cavity if a laser is operating in the anomalous total cavity dispersion regime [10]. Haboucha *et al.* had proposed that the overdrive effect of nonlinear polarization evolution plays a key role in the multipulse evolution [19]. Using the NPR technique, Komarov *et al.* theoretically studied the multipulse and hysteresis phenomena in PML fiber lasers operating in the anomalous and normal dispersion regimes [11]. Wise *et al.* reported that the generation of ultrashort optical pulses tends to be limited by the accumulation of excessive nonlinear phase shifts [16]. Weill *et al.* employed the statistical light-mode dynamics theory to explain the multipulse formation in passive mode locking [20]. Bale *et al.* proposed that the spectral filtering effect plays an essential role in the pulse formation in the net- and all-normal-dispersion fiber lasers [21]. Unfortunately, the aforementioned theories and models may fail to explain our experimental observations for which a laser alternately evolves on the stable and unstable mode-locking states as a function of the pump power P. For example, for $P \approx 45$ mW, our laser is stable mode locked so that the pulses in the temporal and spectral domains are stably shaped without fluctuation. Successively, for $P \approx 62$ mW, it is unstable mode locking that causes the pulses in the temporal and spectral domains to fluctuate strongly without the steady-state pulse shaping. For $P \approx 74$ mW, the laser is stable mode locked again.

In this paper, a theoretical model for describing net- and all-normal-dispersion PML fiber lasers has been proposed by taking into account the NPR mechanism and spectral filtering effect. Numerical simulations on multipulse formation in a PML fiber laser have been presented. The experimental observations have confirmed the theoretical predictions.

II. MODEL AND EQUATIONS

A. Model of laser cavity

A large variety of cavity designs has been proposed to construct PML lasers. The most attention has been focused on cavity dispersion management. The principle of dispersion management has led to the concepts of stretched-pulse [7,22], parabolic-pulse [23], and all-normal-dispersion lasers [16]. The design of laser cavities for higher-energy laser outputs feature the total cavity dispersion shifted into the normal regime.

The proposed DS fiber laser oscillator is shown schematically in Fig. 1. The laser cavity consists of a polarization-sensitive isolator (PS-ISO), two sets of polarization controllers (PCs), a fused coupler, a wavelength-division multiplexing coupler, and a piece of erbium-doped fiber (EDF). The total

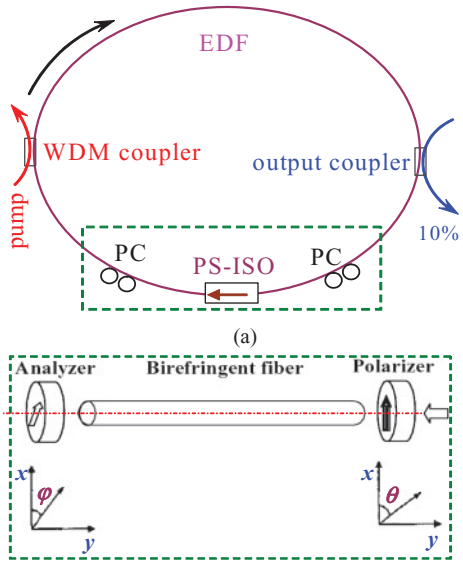

FIG. 1. (Color online) (a) Schematic diagram of DS laser cavity through NPR element (dashed rectangle), and (b) an equivalent setup of the NPR element for determining the cavity transmission. EDF, erbium-doped fiber; WDM, wavelength-division multiplexing; PC, polarization controller; PS-ISO, polarization-sensitive isolator.

length of the laser cavity is about 24 m, including EDF of about 20 m and single-mode fiber (SMF) of about 4 m. The former has a dispersion parameter of $\beta_2 \approx 55 \times 10^{-3}$ ps^2/m at 1550 nm and the latter has a dispersion parameter of about -22×10^{-3} ps^2/m. Then the long EDF provides a large net cavity dispersion of about $+1$ ps^2 to a laser system. The gain medium of EDF has a gain bandwidth of 25 nm and its normalized spectral profile is expressed as [24]

$$g_{\mathrm{nor}}(\omega) = 1/[1 + (\omega/\Delta\omega)^n], \tag{1}$$

where ω and $\Delta\omega$ are the frequency detuning and the EDF bandwidth, respectively, and n is the parameter that determines the flatness of the gain profile (here $n = 6$).

A polarization additive-pulse mode-locking (PAPM) element is made of a PS-ISO and two sets of PCs [the dashed rectangle of Fig. 1(a)]. The intensity transmission of light through a PAPM element is determined by the polarization of polarizer and analyzer together with the linear and nonlinear phase delay. The schematic diagram is shown in Fig. 1(b). The polarizer and analyzer have an orientation of angle θ and φ with respect to the fast axis of the fiber, respectively. Then the intensity transmission of light through the PAPM, T, is expressed as

$$T = \sin^2(\theta)\sin^2(\varphi) + \cos^2(\theta)\cos^2(\varphi) + 0.5\sin(2\theta)\sin(2\varphi)\cos(\phi_1 + \phi_2), \tag{2}$$

where ϕ_1 is the phase delay caused by the polarization controllers and ϕ_2 is the phase delay resulting from the fiber, including both the linear phase delay and the nonlinear phase delay. The PAPM element can effectively clean up and cut off the trailing edges of the pulse. An example is shown in Fig. 2.

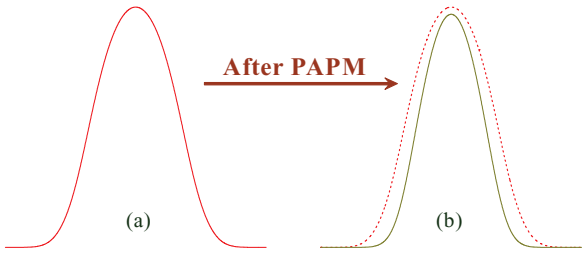

FIG. 2. (Color online) Illustration (a) before and (b) after PAPM effect on pulses in the temporal domain.

The PAPM element is assumed to have a super-Gaussian transmission function with 70-nm bandwidth. Both EDF and PAPM can serve as the spectral filtering elements, which can cut off the temporal wings of a pulse [16,21].

B. Equations and simulations

Usually, the light-wave propagation in the weakly birefringent fibers is modeled by the two coupled equations that involve a vector electric field. For an undoped fiber, the amplitudes of the pulse envelope are found to satisfy the following set of two coupled-mode equations [25]:

$$\frac{\partial u}{\partial z} = -\frac{\alpha}{2}u - \beta_{1x}\frac{\partial u}{\partial t} - i\frac{\beta_2}{2}\frac{\partial^2 u}{\partial t^2} + i\gamma\left(|u|^2 + \frac{2}{3}|v|^2\right)u + i\frac{\gamma}{3}v^2u^*\exp(-2i\Delta\beta z), \tag{3a}$$

$$\frac{\partial v}{\partial z} = -\frac{\alpha}{2}v - \beta_{1y}\frac{\partial v}{\partial t} - i\frac{\beta_2}{2}\frac{\partial^2 v}{\partial t^2} + i\gamma\left(|v|^2 + \frac{2}{3}|u|^2\right)v + i\frac{\gamma}{3}u^2v^*\exp(2i\Delta\beta z), \tag{3b}$$

where u and v denote the envelopes of the optical pulses along the two orthogonal polarization axes of the fiber, and α is the loss coefficient of the fiber. The modal birefringence of the fiber is given by $\Delta\beta = \beta_{0x} - \beta_{0y}$, where β_{0j} is the propagation constant ($j = x, y$); β_{1x} and β_{1y} are the group velocities of the two polarization components, β_2 represents the fiber dispersion, and γ refers to the cubic refractive nonlinearity of the medium. The variables t and z indicate the pulse local time and the propagation distance, respectively.

When waves propagate through EDF, the gain can be included in Eq. (3) by replacing α by $\alpha - g$. In this work, the fiber length L is much larger than its beat length, L_B (here $L \approx 24$ m and $L_B \approx 1$ m). The last terms in Eqs. (3a) and (3b) (i.e., the four-wave-mixing terms) depend crucially on the value of the beat length, L_B ($\Delta\beta = 2\pi/L_B$). For $L \gg L_B$, the four-wave-mixing terms are usually considered negligible because they change sign often and their contribution averages out to zero [25]. For EDF, therefore, the amplitudes of the pulse envelope can be achieved by solving the following equations [25,26]:

$$\frac{\partial u}{\partial z} = -\frac{\alpha}{2}u - \delta\frac{\partial u}{\partial T} - i\frac{\beta_2}{2}\frac{\partial^2 u}{\partial T^2} + i\gamma\left(|u|^2 + \frac{2}{3}|v|^2\right)u + \frac{g}{2}u + \frac{g}{2\Omega_g^2}\frac{\partial^2 u}{\partial T^2},$$

$$\frac{\partial v}{\partial z} = -\frac{\alpha}{2}v + \delta\frac{\partial v}{\partial T} - i\frac{\beta_2}{2}\frac{\partial^2 v}{\partial T^2} + i\gamma\left(|v|^2 + \frac{2}{3}|u|^2\right)v + \frac{g}{2}v + \frac{g}{2\Omega_g^2}\frac{\partial^2 v}{\partial T^2}. \quad (4)$$

Here Ω_g is the bandwidth of the laser gain, $\delta = (\beta_{1x} - \beta_{1y})/2$ is the group velocity difference between the two polarization modes, $T = t - (\beta_{1x} + \beta_{1y})z/2$, and g describes the gain function of EDF and is expressed by [26]

$$g = g_0 \exp(-E_p/E_s), \quad (5)$$

where g_0 is the small signal gain coefficient, related to the doping concentration, and E_s is the gain saturation energy, which is pump-power dependent [27,28]. The pulse energy E_p is given by

$$E_p = \int_{-T_R/2}^{T_R/2} (|u|^2 + |v|^2)\, d\zeta, \quad (6)$$

where T_R is the cavity round-trip time.

The light transmission through fibers can be simulated by solving Eqs. (3) or (4) and by using the spectral filtering. The implementation of the numerical simulation is described as follows in detail. The fiber length is divided into a lot of segments and the pulse is propagated from segment to segment. The optical field is first propagated for a distance of $h/2$ and the simulation is operated in the spectral domain. Successively, the spectral filtering is implemented by the gain bandwidth of EDF if the pulses are propagated through EDF. At the midplane, $z + h/2$, the field is multiplied by a nonlinear term in the temporal domain. Then the field is simulated in the spectral domain when it is propagated the remaining distance, $h/2$. Finally, the spectral filtering via the gain bandwidth of EDF is operated. The implementation of spectral filtering is ignored if the pulse is propagated through the undoped fiber. Therefore, the proposed numerical model incorporates the most important physical effects such as the NPR, spectral filtering, GVD, and the Kerr effect.

In comparison with the numerical models proposed by Tang *et al.* [10], Komarov *et al.* [11], and so on, the proposed model here takes into account the spectral filtering effects induced by the gain bandwidth of EDF and the transmission bandwidth of PAPM.

III. SIMULATION RESULTS

Numerical simulations show that, by appropriately setting the polarization of polarizer and analyzer and the linear cavity phase-delay bias of the cavity, self-started mode locking can be achieved. Since the saturation energy E_s is proportional to the pumping strength [28], increasing E_s corresponds to increasing the pump power in the experiments. We use the following parameters for our simulations for possibly matching the experimental conditions: $\alpha = 0.2$ dB/km, $g_0 = 3\ \mathrm{m}^{-1}$, $\gamma = 4.5\ \mathrm{W}^{-1}\ \mathrm{km}^{-1}$ for EDF and $1.3\ \mathrm{W}^{-1}\ \mathrm{km}^{-1}$ for SMF, $\Omega_g = 25$ nm, $\theta = \pi/3.9$, $\varphi = \pi/5$, $\phi_1 = 0.3 + \pi/2$, $\beta_2 = +55 \times 10^{-3}\ \mathrm{ps}^2/\mathrm{m}$ for EDF and $-22 \times 10^{-3}\ \mathrm{ps}^2/\mathrm{m}$ for SMF, and the net cavity GVD $\beta_{net} \approx +1\ \mathrm{ps}^2$.

By appropriately setting the angles θ and φ and the phase delay ϕ_1, the DS number over a cavity round-trip time is generated one by one with the increase of the pumping parameter E_s, while the number of pulses disappears one by one for decreasing E_s. The formation and annihilation of each pulse show the pumping parameter hysteresis. The simulation results are shown in Fig. 3, where the dashed and solid segments denote that the laser operates on the unstable and stable mode-locking states, respectively. The thick and thin curves in Fig. 3 represent the ascending and descending pump-strength processes, respectively. In simulations, when the laser system achieves the self-consistent intracavity pulse evolution, the pulses in the temporal and spectral domains are stably shaped and, hence, the laser operates in the stable mode-locking state. However, when the laser works at the unstable mode-locking state, the temporal and spectral profiles of the pulses are strongly fluctuated as shown in Fig. 4.

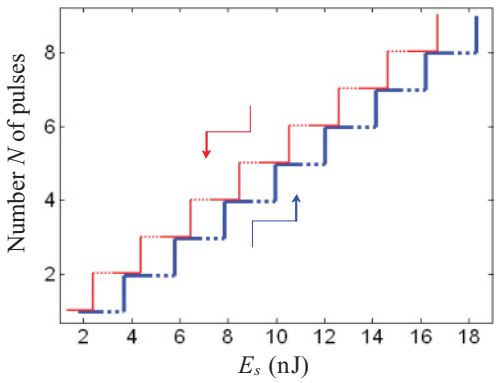

FIG. 3. (Color online) Relationship between the DS number over a round-trip time and the pump strength. The thick and thin curves denote the ascending and descending pump strength, respectively. The solid and dashed segments represent the stable and unstable mode-locking states of the laser, respectively. There is no mode locking for the pump strength $E_s < 1.8$ nJ and $E_s < 1.3$ nJ during the ascending and descending pumping process, respectively, so that the DS number can be considered $N = 0$.

One can observe from Fig. 3 that the stable and unstable mode-locking states of the laser alternately evolve along the pumping strength E_s. Our simulation results are quite different from the results reported in Refs. [10,11], where the mode-locking state stably evolves along the pump strength.

Figure 4 shows some typical results of numerical simulations for the ascending pump process in the single-pulse mode-locking regime. We can observe from Figs. 3 and 4 that (a) there is no mode locking for the pump strength $E_s < 1.8$ nJ when the laser operates on the ascending pump strength process; (b) a mode-locked DS pulse emerges in the cavity from $E_s \approx 1.8$ to 3 nJ; (c) the proposed laser operates unstably from $E_s \approx 3$ to 3.7 nJ; (d) two DS pulses emerge in the cavity when E_s is further increased; and (e) the pulse characteristics periodically evolve as a function of pump strength. Figure 4 exhibits that the spectral width broadens and the pulse duration increases with the increase of pump strength E_s in the single-pulse mode-locking regime. For example, the spectral width $\Delta\lambda$ and the pulse duration $\Delta\tau$ at a full width at half maximum (FWHM) are about 13 nm and 46 ps for $E_s = 2.8$ nJ, respectively, instead of $\Delta\lambda \approx 9$ nm and $\Delta\tau \approx 40$ ps for $E_s = 1.9$ nJ.

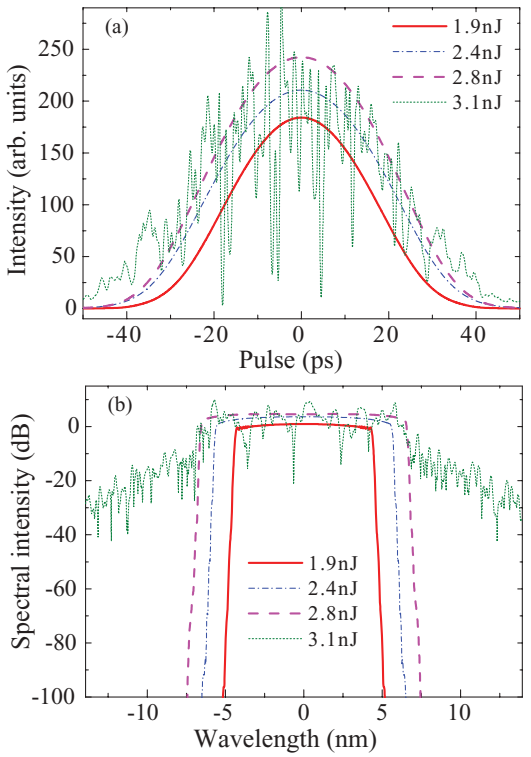

FIG. 4. (Color online) Numerical simulations of (a) temporal intensity profile and (b) spectral intensity profile for different pumping parameter E_s.

IV. EXPERIMENTS AND COMPARISONS

The experimental setup for the laser oscillator of producing DSs matches the simulated arrangement as shown in Fig. 1. EDF provides the gain amplification for the laser system pumped by a 977-nm laser diode. An autocorrelator, optical spectrum analyzer, and 11-GHz oscilloscope together with a 12-GHz photodetector are used to simultaneously monitor the laser output. The cavity has the dispersion map with normal and anomalous GVD of about $+1.1$ and -0.1 ps^2, respectively. The proposed laser cavity has very large net-normal GVD and thus it would presumably have to exploit dissipative processes in the mode-locked pulse shaping [16].

By adjusting two polarization controllers with appropriate orientation and pressure settings, self-started mode locking of the laser is achieved at the threshold pump power $P \approx 44.8$ mW. Figures 5(a)–5(c) show the optical spectrum of the pulses and the corresponding autocorrelation and oscilloscope traces, respectively. The optical spectrum has steep spectral edges but no sharp peaks near its edges. The experimental observations are in excellent agreement with the simulation results, as shown in Fig. 4(b). Both experimental and numerical results are different from the typical spectrum characteristics of all-normal-dispersion lasers where there are steep spectral edges and sharp peaks on the edges.

It is seen from Fig. 5 that (i) the spectral width $\Delta\lambda$ of solitons is about 10.3 nm; (ii) the autocorrelation trace has a FWHM of about 63 ps (corresponding to the pulse duration of $\Delta\tau \approx 45$ ps); and (iii) the pulse separation is about 115 ns, corresponding to the fundamental cavity frequency ~8.7 MHz [Fig. 5(c)].

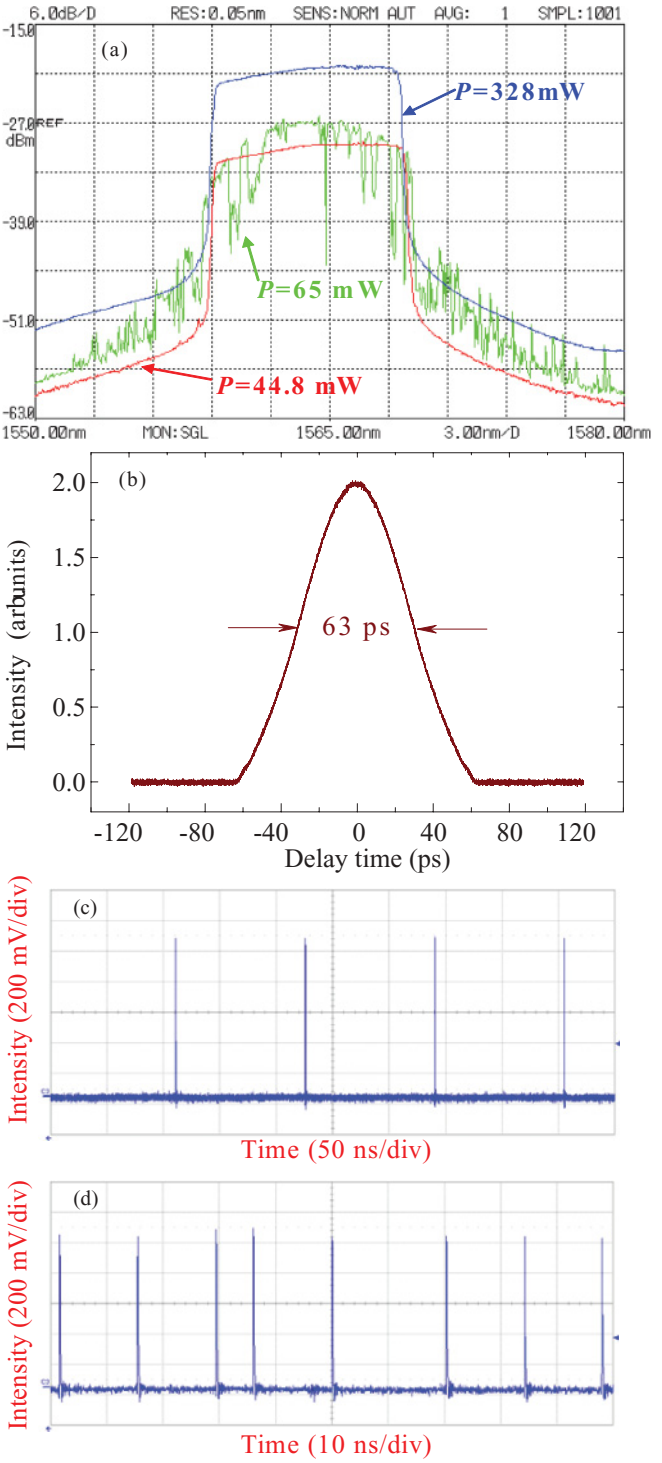

FIG. 5. (Color online) (a) Optical spectra of pulses, (b) autocorrelation trace, (c) oscilloscope trace at pump power $P = 44.8$ mW for single-pulse operation, and (d) oscilloscope trace at $P = 328$ mW for eight-pulse operation. The laser operates in the stable mode-locking state for $P = 44.8$ and 328 mW and the unstable mode-locking state for $P = 65$ mW.

From enhancing the pump power, the experimental observations show that the fiber laser stably emits pulses with an increase of the pulse duration and spectral width. These results agree well with the numerical simulation shown in

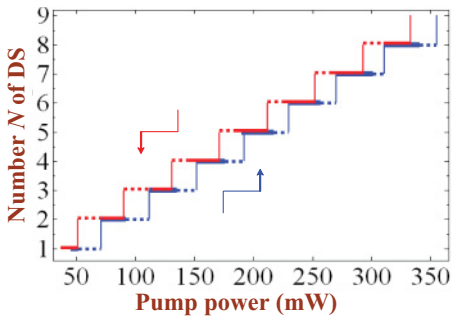

FIG. 6. (Color online) Experimental observations of the DS number N as a function of the pump power P. The solid and dashed segments denote the stable and unstable mode-locking states of the laser, respectively. The stepwise-up and stepwise-down curves refer to the ascending and descending pump-power processes, respectively.

Figs. 4(a) and 4(b). However, the laser operates unstably when the pump power P is from ~52.4 to ~71.3 mW. An experimental example at $P = 65$ mW is shown in Fig. 5(a). The laser emits two DS pulses over a cavity round-trip time from $P \approx 71.3$ to 96 mW. The experimental observations demonstrate that the proposed laser alternately evolves on the stable and unstable mode-locking states as a function of the pump power. The experimental results are shown in Fig. 6 in detail, where the stepwise-up and stepwise-down curves refer to the ascending and descending pump power processes, respectively. The solid and dashed segments denote the stable and unstable mode-locking states of the laser, respectively.

For $P \approx 328$ mW, there are eight DS pulses coexisting in the cavity. The spectral profile and the oscilloscope traces are shown in Figs. 5(a) and 5(d), respectively. We can see from Figs. 5(c) and 5(d) that the pulse height in the eight-pulse regime is approximately the same as that in the single-pulse regime. Since the measured pulse height in the oscilloscope trace is directly related to the energy of each individual pulse [10], the pulses at $P = 44.8$ and 328 mW have approximately the same pulse width and pulse energy. Actually, the autocorrelation traces at $P = 328$ mW are similarly to that in Fig. 5(b).

It is seen from Fig. 6 that the laser operates on the unstable mode-locking state when the pump power P is decreased to a certain value. If P is further decreased, the laser is in the stable mode-locking state again, whereas the number of pulses disappears one by one over a cavity round-trip time. This occurs until the laser becomes continuous. The dynamics for descending pump power is different from that for ascending pump power. As a result, hysteresis phenomena occur as a function of pump power. These experimental observations agree well with the theoretical predictions, as shown in Fig. 3.

According to Tang's theory [10], the pump-power hysteresis of the pulse operation of the laser is caused by the existence of the linear cavity loss of a practical laser. The stronger the linear cavity loss, the greater is the pump hysteresis of the pulse operation. The theoretical results achieved by Komarov and Tang *et al.* [10,11] show that the more pulses that exist in the cavity, the bigger the hysteresis. However, our numerical and experimental results (Figs. 3 and 6) demonstrate that the pump-power hysteresis is approximately independent of the pulse number of the laser cavity. The simulation results suggest that the spectral filtering effect plays a key role in the difference between our results and the reported results in Refs. [10,11].

V. QUALITATIVE EXPLANATION OF MULTIPULSE FORMATION AND EVOLUTION

One can see from Fig. 1(b) and Eq. (2) that the cavity transmission of the laser cavity is a sinusoidal function of the phase delay with a period of 2π. When the orientation of the polarizer and analyzer have certain fixed angles of θ and φ, respectively, the laser cavity supplies positive cavity feedback only in half of the period, whereas it supplies negative cavity feedback in the other half of the period. It is found from Eq. (2) that, with an appropriate selection of the phase delay ϕ_1, the cavity feedback can be switched from the positive to the negative feedback regime when the nonlinear phase delay is increased. When the pump strength is enhanced, the peak power of pulses is increased [an example is shown in Fig. 4(a)] and then the nonlinear phase delay is also increased. When the peak power of pulses is so strong that it can switch the cavity from the positive to the negative feedback regime, a further increase of the pulse peak power results in which the actual cavity transmission that the pulse experiences becomes smaller than the linear cavity transmission. In this case, the background noise is more amplified than the pulse. Then the background noise starts to lase with a certain frequency and form a continuous wave (CW) component in the pulse spectrum. An example of experimental observations is shown in Fig. 7 (see the curve labeled $P = 55$ mW). At the same time, the spectral filtering effect induced by the gain bandwidth of EDF can effectively enhance the modulation instability. The modulation instability of linear waves together with the spectral filtering effect causes the laser cavity to be in unstable operation. With the increase in pump strength, the unstable operation is enhanced. An experimental example is exhibited in Fig. 7 (see the curve labeled $P = 62$ mW). After a further increase in the pump power, the strongest linear wave becomes modulated and is shaped into an additional pulse, and hence the laser is in stable mode-locking operation again. Figure 7 shows an example at pump power $P = 74$ mW. As this happens, all pulses in the cavity appropriately adjust their energy because of the nergy balance. As a result, the peak intensities of these pulses

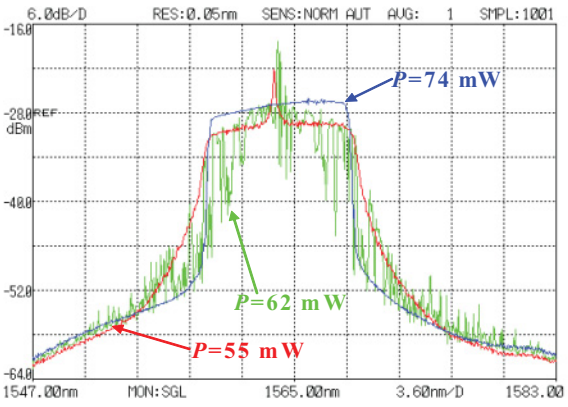

FIG. 7. (Color online) Optical spectra of laser at pump power $P = 55$, 62, and 74 mW.

are decreased. After further enhancing the pump strength, the peak intensities of these pulses are increased and then the aforementioned process repeats again. These processes explain the lower stepwise curve in Figs. 3 and 6. The theoretical analysis exactly matches the experimental observations of how an additional pulse is generated (see the curves labeled $P = 44.8$, 55, 62, 65, and 74 mW in Figs. 5 and 7).

In the case of a multipulse operation with reducing pump strength, the peak intensity of pulses is decreased. In this case, we assume that the laser emits N pulses over a cavity round-trip time. When the pump power is decreased to a certain value, the pumping energy may not drive the N-pulse mode-locking operation because the balance between the energy being supplied and the energy lost has to be exact in the dissipative system. Then the laser changes to the unstable operation due to the combined effects of the modulation instability of linear waves and the spectral filtering effect of the EDF gain bandwidth. After a further decrease in the pump power, the energy of the linear waves is below the threshold of the modulation instability. At this state, the CW component and pulses coexist in the cavity. If the pump power is further decreased to another certain value, the appropriate pumping energy can support the $(N-1)$-pulse operation. As a consequence of the energy balance between that in the supply and that lost in the dissipative system, the laser operates in the $(N-1)$-pulse mode-locking regime. The aforementioned process explains the upper stepwise curve in Figs. 3 and 6.

VI. CONCLUSIONS

A theoretical model describing the multipulse DS evolution in net-normal-dispersion PML fiber lasers is proposed in this paper. The model is based on the NPR technique and the spectral filtering mechanism, including the most important physical effects such as GVD, spectral filtering, and the Kerr effect. It is numerically found and experimentally observed that the net-normal-dispersion PML laser alternately evolves over the stable and unstable mode-locking states as a function of the pump strength. Numerical simulations and experimental observations show that the DS pulses in the cavity appear or disappear one by one when the pump is increased or decreased, respectively, and that large pump strength hysteresis exists. The multistability and hysteresis phenomena observed in this laser are quite different from those observed in conventional soliton fiber lasers [10,11]. These anomalous behaviors can be explained as a consequence of the combined action of the NPR mechanism and the spectral filtering effect.

ACKNOWLEDGMENTS

This work was supported by the "Hundreds of Talents Programs" of the Chinese Academy of Sciences and by the National Natural Science Foundation of China under Grant Nos. 10874239 and 10604066. The author would especially like to thank Leiran Wang, Xiaohui Li, and Yongkang Gong for help with the experiments.

[1] A. Haboucha, H. Leblond, M. Salhi, A. Komarov, and F. Sanchez, Phys. Rev. A **78**, 043806 (2008).
[2] J. M. Soto-Crespo, M. Grapinet, P. Grelu, and N. Akhmediev, Phys. Rev. E **70**, 066612 (2004).
[3] S. Masuda, S. Niki, and M. Nakazawa, Opt. Express **17**, 6613 (2009).
[4] M. Salhi, A. Haboucha, H. Leblond, and F. Sanchez, Phys. Rev. A **77**, 033828 (2008).
[5] B. Vodonos, R. Weill, A. Gordon, A. Bekker, V. Smulakovsky, O. Gat, and B. Fischer, Phys. Rev. Lett. **93**, 153901 (2004).
[6] A. Zavyalov, R. Iliew, O. Egorov, and F. Lederer, Phys. Rev. A **79**, 053841 (2009).
[7] K. Tamura, E. P. Ippen, H. A. Haus, and L. E. Nelson, Opt. Lett. **18**, 1080 (1993).
[8] L. A. Gomes, L. Orsila, T. Jouhti, and O. G. Okhotnikov, IEEE J. Sel. Top. Quantum Electron. **10**, 129 (2004).
[9] A. B. Grudinin, D. J. Richardson, and D. N. Payne, Electron. Lett. **28**, 67 (1992).
[10] D. Y. Tang, L. M. Zhao, B. Zhao, and A. Q. Liu, Phys. Rev. A **72**, 043816 (2005).
[11] A. Komarov, H. Leblond, and F. Sanchez, Phys. Rev. A **71**, 053809 (2005).
[12] J. M. Soto-Crespo and Nail Akhmediev, Phys. Rev. Lett. **95**, 024101 (2005).
[13] N. Akhmediev and A. Ankiewics, Eds. *Dissipative Solitons* (Springer, Berlin-Heidelberg, 2005).
[14] W. H. Renninger, A. Chong, and F. W. Wise, Phys. Rev. A **77**, 023814 (2008).
[15] W. Chang, A. Ankiewicz, J. M. Soto-Crespo, and N. Akhmediev, Phys. Rev. A **78**, 023830 (2008).
[16] F. W. Wise, A. Chong, and W. Renninger, Laser Photon. Rev. **2**, 58 (2008).
[17] A. Komarov and F. Sanchez, Phys. Rev. E **77**, 066201 (2008).
[18] W. Chang, J. M. Soto-Crespo, A. Ankiewicz, and N. Akhmediev, Phys. Rev. A **79**, 033840 (2009).
[19] A. Haboucha, A. Komarov, H. Leblond, F. Sanchez, and G. Martel, Opt. Fiber. Technol. **14**, 262 (2008).
[20] R. Weill, B. Vodonos, A. Gordon, O. Gat, and B. Fischer, Phys. Rev. E **76**, 031112 (2007).
[21] B. G. Bale, J. N. Kutz, A. Chong, W. H. Renninger, and F. W. Wise, J. Opt. Soc. Am. B **25**, 1763 (2008).
[22] V. Roy, M. Olivier, F. Babin, and M. Piché, Phys. Rev. Lett. **94**, 203903 (2005).
[23] F. O. Ilday, J. R. Buckley, W. G. Clark, and F. W. Wise, Phys. Rev. Lett. **92**, 213902 (2004).
[24] W. S. Man, H. Y. Tam, M. S. Demokan, P. K. A. Wai, and D. Y. Tang, J. Opt. Soc. Am. B **17**, 28 (2000).
[25] G. P. Agrawal, *Nonlinear Fiber Optics*, 4th ed. (Academic Press, Boston, 2007).
[26] G. P. Agrawal, IEEE Photonics Technol. Lett. **2**, 875 (1990).
[27] A. Cabasse, B. Ortaç, G. Martel, A. Hideur, and J. Limpert, Opt. Express **16**, 19322 (2008).
[28] G. Martel, C. Chédot, V. Réglier, A. Hideur, B. Ortaç, and Ph. Grelu, Opt. Lett. **32**, 343 (2007).